Conference Paper, Published Version

Stößer, T.; Rodi, Wolfgang; Jirka, Gerhard H.

Large-Eddy Simulation of Flow over Rough Channel Beds (Large Eddy Simulation der Strömung über rauen Sohlen)

11 Large-Eddy Simulation of Flow over Rough Channel Beds

Large Eddy Simulation der Strömung über rauen Sohlen

T. Stößer, W. Rodi, G. Jirka

Institute for Hydromechanics, University of Karlsruhe, Germany
Institut für Hydromechanik, Universität Karlsruhe

ABSTRACT: In this paper we show the results of large eddy simulations (LES) of the flow in a closed channel where one wall is roughened with square bars or circular rods respectively. Whereas the roughness height *k* is kept at *0.2* of the half channel depth, the spacing between the elements *w* is varied from *w/k=3* to *w/k=10*, covering the range of d-type (quasi-smooth flow), transitional (wake interference) and k-type (isolated) roughness. The structure of turbulence as well as the statistical quantities exhibit differences for the different roughness types. For d-type roughness the separation zones behind the elements are confined to the cavities, and only a few turbulent eddies are shed into the outer flow. For transitional and k-type roughness, separation and reattachment occur between two adjacent bars/rods and much larger and more frequent eddies are found. For the evaluation of coherent structures and for the quantification of the four events of the bursting phenomena a quadrant-analysis is used. It is shown that for the turbulent fluctuations sweeps and ejections near the roughness elements are dominant irrespective of their shape and the spacing between them. Another feature of turbulent wall bounded flows is the formation of high and low speed streaks. Although streaks form above all types of roughness, their size and shape are different for each roughness configuration.

KURZFASSUNG: In diesem Beitrag zeigen wir die mit der Methode der Large Eddy Simulationen (LES) berechnete Strömung in einem geschlossenen Kanal bei dem eine Wand mit Rauheitsstreifen besetzt wurde. Die Rauheitshöhe *k* wurde zu *0.2* der halben Kanalhöhe gewählt, der Abstand *w* zwischen den Rauheitstreifen wurde von *w/k=3* bis *w/k=10* so variiert, dass die drei Rauheitstypen „d-type (quasi-smooth flow)“ , „transitional (wake interference)“ und „k-type (isolated) roughness“ abgedeckt sind. Die Struktur der Turbulenz sowie die Statistik der Strömung zeigen deutliche Unterschiede für die drei Rauheitstypen. Für die “d-type roughness” füllt die Ablösezone hinter den Elementen vollständig den Zwischenraum aus und nur wenige Wirbel werden in die Außenströmung geschleudert. Für “transitional” und “k-type” Rauheiten, findet das Wirbelablösen und das Wiederanlegen zwischen zwei Rauheitselementen statt und größere und häufiger auftretende Wirbel werden gelöst. Bei der Auswertung der auftretenden kohärenten Strukturen wird die Quadranten Analyse verwendet. Es wird gezeigt, dass sogenannte “sweeps” und “ejections” in der Nähe der Rauheitsstreifen dominieren und zwar unabhängig von der Form der Streifen bzw. des Abstands zwischen diesen. Ein weiteres Phänomen der Gerinneströmung ist die Bildung von “high“ und „low speed streaks“. Obwohl diese sich über allen Rauheitstypen formieren variieren sie doch in Abhängigkeit der jeweiligen Konfiguration.

11.1 Introduction

Turbulent boundary layers over roughness elements have considerable engineering interest. Especially in the field of hydraulic engineering, nearly all practical flows are hydraulically rough, i.e. the roughness Reynolds number $Re_* = (u_\tau k)/\nu$ (where u_τ is the friction velocity, k is a characteristic roughness height and ν is the kinematic viscosity) exceeds a certain value ($Re_* > 70$) and the roughness affects the flow outside the roughness sublayer. Following the classification of /Morris 1955/ the effect of roughness is mainly due to the formation of wakes behind the roughness elements resulting in the production of turbulence and the dissipation of energy. According to Morris the ratio of longitudinal spacing w to the roughness height k is of paramount importance in rough wall channel flow, classifying the roughness into three basic types (Figure 11-1): isolated roughness flow (k-type), wake interference flow (transitional) and quasi-smooth flow (d-type).

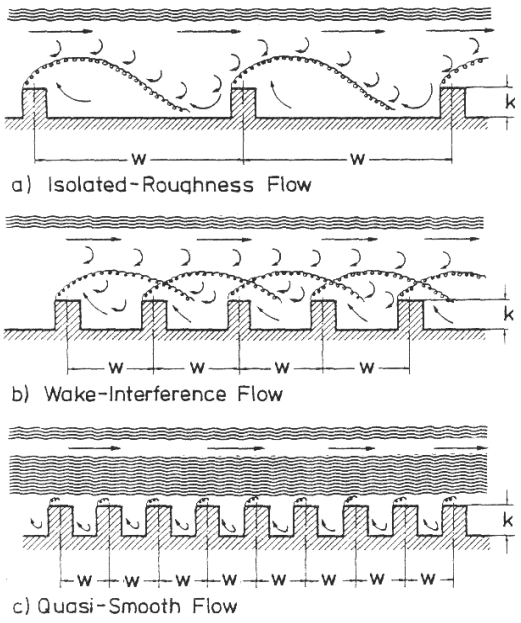

Figure 11-1 Roughness types in rough wall channel flow according to /Morris 1955/

The mean velocity profiles in channels over rough beds differ considerably from the profile over a smooth bed (e.g. /Patel 1998/) since the surface drag is significantly larger when roughness elements are present. However, the effect of roughness is not restricted to the mean flow properties. Flow visualizations and measurements (e.g. /Grass 1971/, /Grass et al. 1991/, /Djenidi et al. 1999/ and many others) as well as recent DNS calculations of flow over rough-walls (/Leonardi et al. 2003/, /Miyake et al. 2002/) indicate significant structural changes not only near the rough surface, but everywhere within the boundary layer. The presence of organized structures near the walls, which are mainly responsible for the transport of momentum, heat and mass across the boundary layer /Grass 1971/ is, irrespective of surface condition, established from these research endeavours. The streamwise velocity field near rough walls is, similar to the velocity field over smooth walls, organized into alternating narrow streaks of high and low speed fluid that are persistent, vary only slowly, and exhibit a preferential spanwise spacing /Grass et al. 1991/. However, /Leonardi et al. 2003/ have shown that due to surface roughness, size and shape of coherent streaks change drastically as a result of enhanced momentum exchange between the near-wall region and the outer flow. Most turbulence production occurs when the low speed streaks are lifted away from the wall-layer in a violent ejection and during inrushes of high speed fluid from the outer layer back towards the wall. The complete cycle of lift-up of fluid, ejection and sweep motion makes up what is usually called the bursting phenomenon (see papers e.g. by /Kline et al. 1967/, /Corino & Brodkey 1969/, or the summary by /Robinson 1991/). Since the late 1960's intensive experimental research on these mechanisms has been conducted in order to shed light on the bursting phenomenon and the associated structures occurring over smooth and rough walls by means of different techniques. Flow visualisations of streaky patterns through passive tracers (e.g. /Defina 1996/ or hydrogen bubbles were used /Grass et al. 1991/ in order to study qualitatively the bursting processes. More quantitatively, different conditional sampling techniques were applied in order to detect coherent structures from velocity fluctuation signals. Among these, the quadrant analysis by /Lu & Willmarth 1973/ is to date the most popular and probably the most used. The streamwise and wall-normal velocity fluctuations u' and w' are divided into four quadrants in order to evaluate the contributions of ejections and sweeps to the Reynolds stress. The definition and terminology of "sweeps" with $u'>0,\ w'<0$, "ejections" with $u'<0,\ w'>0$, "inward interaction" with $u'<0,\ w'<0$ and "outward interaction" with $u'>0,\ w'>0$ is since then applied systematically.

In this paper we show the results of several large-eddy simulations (LES) of channel flow over a bed artificially roughened by both square-bar and circular-rod elements for the above mentioned three roughness types. The main purpose of this study is to provide further insight into the turbulent flow over rough boundaries and to enhance the understanding of the effect of surface roughness geometry on the mean and instantaneous flow. Temporal averaging is used to quantify the effects of the three roughness types with regard to flow velocities, turbulent fluctuations and Reynolds stresses. Furthermore, we investigate the occurrence of coherent flow structures in dependence on the nature of the

roughness and compare them to the equivalent structures on a smooth wall.

11.2 Numerical Methodology

Two LES codes, LESOCC developed at the Institute for Hydromechanics, University of Karlsruhe /Breuer & Rodi 1996/ and MGLET, developed at the Institute for Fluidmechanics at Technical University of Munich /Tremblay & Friedrich 2001/, are used to perform the large-eddy simulations. Both codes solve the filtered Navier-Stokes equations discretised with the finite volume method. Whereas MGLET is based on a staggered Cartesian grid, LESOCC allows the use of a non-staggered grid on curvilinear coordinates. In both codes convective and diffusive fluxes are approximated with central differences of second order accuracy. The Poisson equation for coupling the pressure to the velocity field is solved with the SIP method of /Stone 1968/. Time advancement is achieved by a second order, explicit Runge-Kutta scheme in LESOOC and a by second order, explicit Adams-Bashford scheme in MGLET, respectively. The subgrid-scale stresses appearing in the filtered Navier-Stokes equations are computed using the dynamic approach of /Germano et al. 1991/. The no-slip boundary condition is used on all walls including the surface of the roughness elements. The treatment of the square and circular elements needs special attention. The square bars are represented by the discrete-element technique, such that the boundaries of the bars coincide with the grid lines and the “inner” cells of the bar are blocked out from the computation. This technique cannot be applied without difficulty to the round-shaped rods, as it would require a fairly complex curvilinear, multi-block grid. A much simpler way but similarly accurate of treating arbitrarily shaped bodies is to use a Cartesian grid together with the immersed boundary method, a technique already invented in the seventies by /Peskin 1972/ and then followed by many others (e.g. /Verzicco et al. 1996/, /Gullbrand et al. 1997/, /Tremblay & Friedrich 2001/). Whereas the code LESSOC is used for the square bar roughened channel, the code MGLET offers the possibility of using the immersed boundary method and is therefore used for the computation of the rod roughened channel flow.

11.3 Flow Configurations

Three configurations with ratios of $w/k = 10$ (isolated flow), $w/k = 7$ (wake interference flow) and $w/k = 3$ (quasi smooth flow) are selected in order to simulate the three roughness types according to Figure 11-1. The domain size, boundary conditions and the Re number of 4200, based on half channel depth and bulk velocity, are chosen analogous to recent DNS by /Leonardi et al. 2003/, who investigated the flow in a closed channel where one wall was roughened with bars or rods, respectively. This allows us to also carry out a comparison LES - DNS and verify both LES codes used. The roughness Reynolds number Re_τ and the ratio of roughness height to water depth is $k/h=0.2$. The computational domain spans $8h$ in streamwise, πh in spanwise and $2h$ in vertical directions, respectively. Several simulations with different grid resolutions were carried out; however in this paper we will only present the results from the finest grid consisting of 260 x 60 x 120 grid points. The grid spacings in terms of wall units are $\Delta x^+ \approx 13$ in streamwise direction, $\Delta y^+ \approx 21$ in spanwise direction and less than 2 for Δz^+ near the walls and the roughness elements. These are approximately double the mesh sizes than employed in the DNS where the spacings were $\Delta x^+ \approx 8$, $\Delta y^+ \approx 13$ and approximately 1 for Δz^+ near the walls and roughness elements. Periodic boundary conditions were applied in the streamwise and spanwise directions. The no-slip boundary condition was used on and between the roughness elements, representing the rough lower wall, as well as on the smooth upper wall.

11.4 Results and Discussion

11.4.1 Time Averaged Flow Field

Figure 11-2 shows the time-averaged flow field above and around the three roughness types for both bar and rod roughened channels. For the sake of brevity only a few selected configurations are presented. In each figure the results of the DNS calculations of /Leonardi et al. 2003/ are plotted below for comparison.

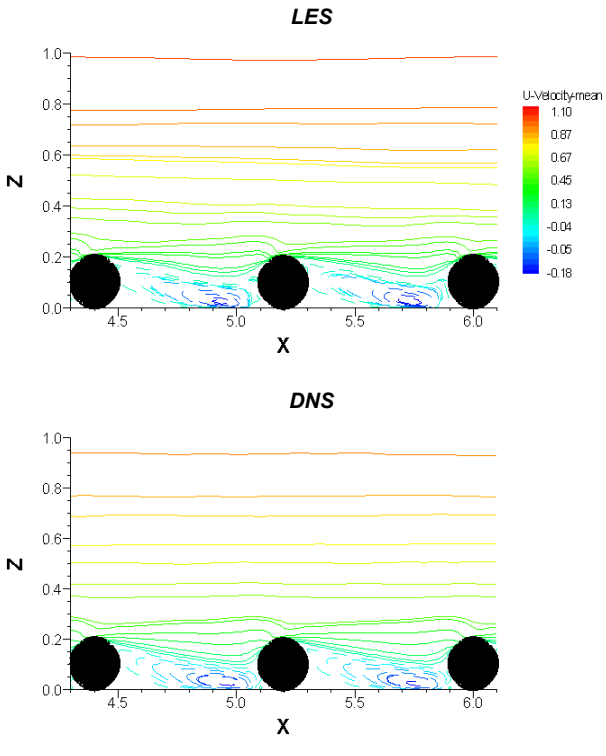

a.) quasi-smooth rod roughness

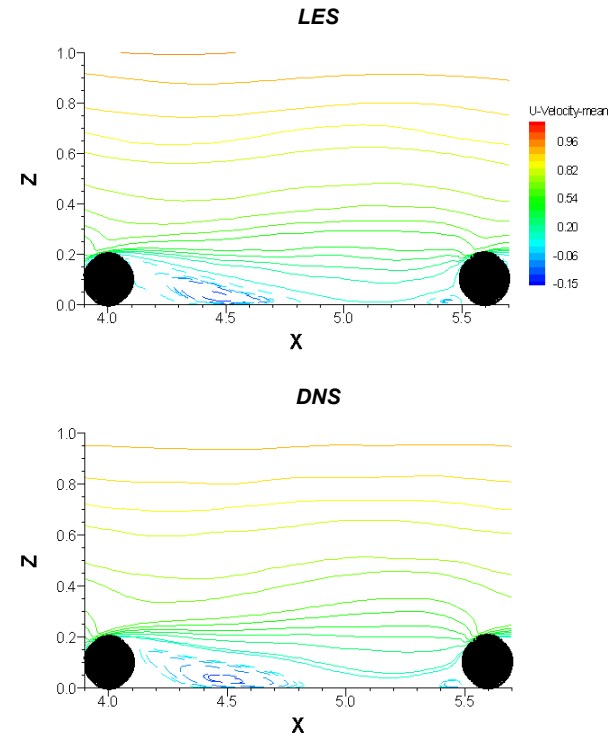

b.) transitional rod roughness

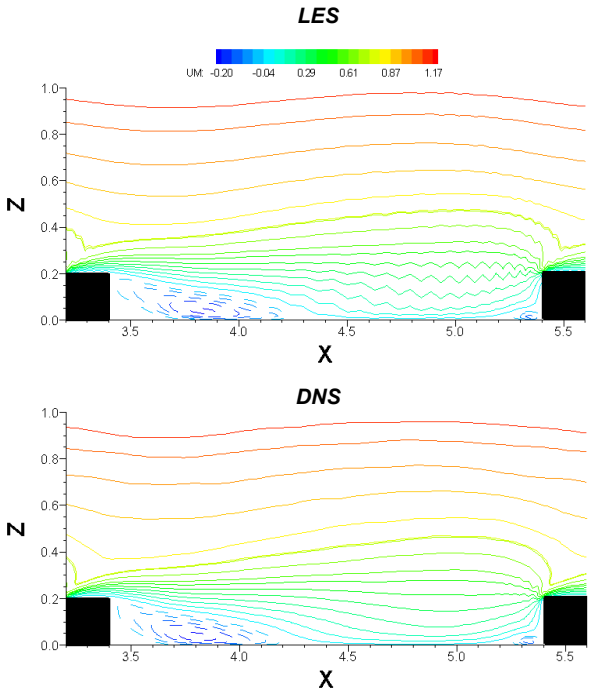

c.) isolated bar roughness

Figure 11-2 Comparison of LES and DNS results for the time and spanwise averaged streamwise velocity u in the vicinity of the circular rods or square bars, respectively for the three roughness types

The flow develops strong separation zones near the roughness elements causing a shear layer above the elements of different extent and a strong disturbance of the flow field in the vicinity of the elements. Whereas for the isolated and transitional roughness the flow reattaches in the trough, the separation zone for the quasi-smooth flow fully occupies the cavity that is formed by the roughness elements. In the latter case, for both rods and bars, the cavity is completely filled with a stable eddy and the streamlines connect the tops of the elements, creating a pseudo-wall. The average flow field undergoes a more or less strong undulation above the roughness elements for transitional and isolated roughness. /Perry et al. 1969/ attributed this roughness-induced streamwise distortion to standing waves, forming just above the roughness elements.

A more homogenous flow field above the crests (similar to a flow field above a smooth wall) appears for the quasi-smooth flow. These features are in good agreement with the sketches given in Figure 11-1. Moreover, the predictions of the LES match very well the results of the DNS. The length and the shape of the recirculation zones are identical as well as the small bubble that is formed in front of the roughness elements for transitional and isolated roughness. A numerical feature is also visible for the sharp crested bar roughness, especially for the transitional and isolated roughness types: due to the standing waves the numerical scheme is prone to wiggles that are present in front of the element, in fact for the LES as well as for the DNS.

Figure 11-3 shows exemplary the distribution of the vertical velocity averaged in time and spanwise direction for both bar and rod type elements.

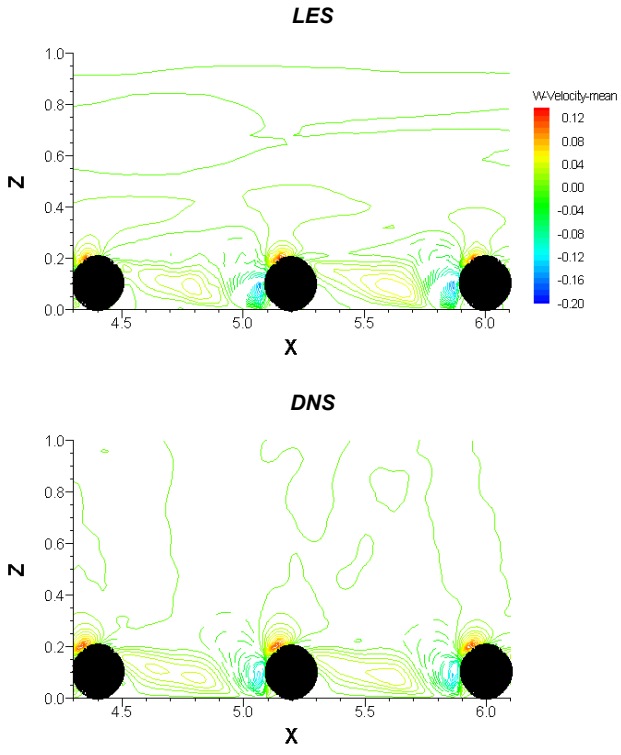

a.) quasi-smooth rod roughness

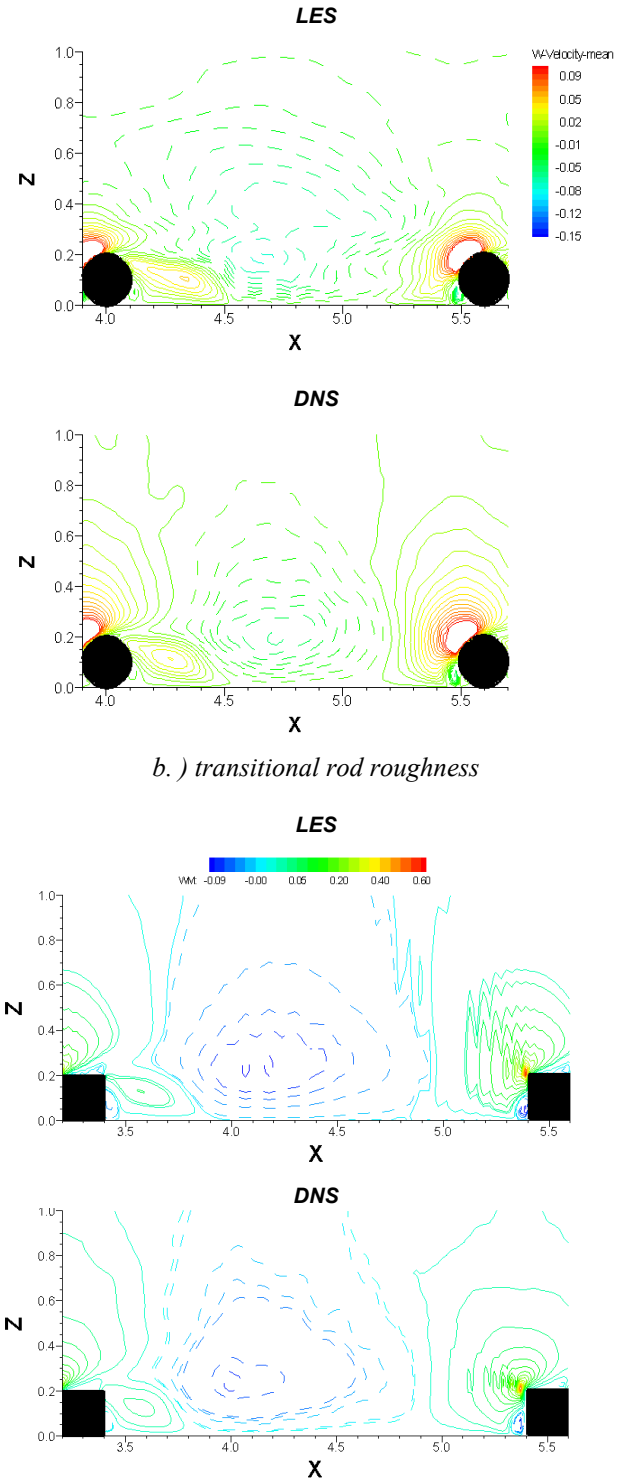

b.) transitional rod roughness

c.) isolated bar roughness

Figure 11-3 Comparison of LES and DNS results for the time and spanwise averaged vertical velocity w in the vicinity of the circular rods or square bars, respectively for the three roughness types

Whereas for the bars a small peak of positive vertical velocities occurs only at the leading edge of the element, the maximum upflow takes place over a larger region at the front of the rods. Also apparent is the much bigger region of negative vertical velocities, indicated by the dashed contour lines, for transitional and isolated roughness in comparison to the quasi-smooth roughness.

Figure 11-4 shows the comparison of mean streamwise velocities for the three types at the top of the element (left) and in the centre of the cavity (right side) for both bar and rod roughness. The figures indicate clearly that the shape of the roughness elements has much less influence than the ratio of element spacing to roughness height *w/k*. The effect of the elements is evident in the shift of the streamwise velocity maximum towards the upper smooth wall. This shift is largest for the transitional and isolated roughness irrespective of element shape.

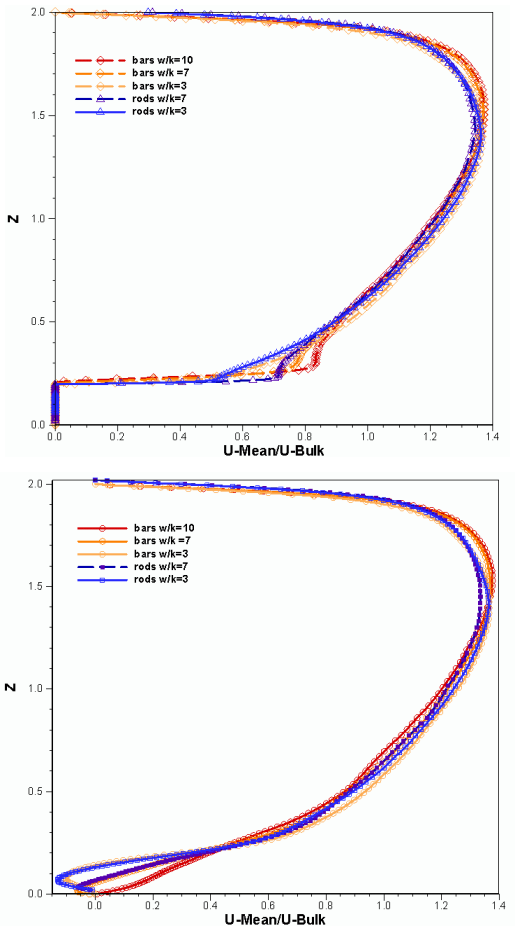

Figure 11-4 Comparison of the time and spanwise averaged streamwise velocity u on the top of each roughness element (upper figure) and in the centre of the groove (lower figure) for the three roughness types

The above mentioned standing waves also affect significantly the turbulence intensity distributions in the vicinity of the rough wall. Figure 11-5 shows the *rms* values of the streamwise velocity fluctuations in the vicinity of the square bars. The comparison with the DNS indicates that the overall prediction of the

second order statistics is in general satisfactory, especially with regard to the position and the magnitude of the maximum values. It is noteworthy, that for the quasi-smooth roughness the maximum streamwise fluctuations occur halfway between the roughness elements whereas for the two other roughness types they are located directly above the top of the elements.

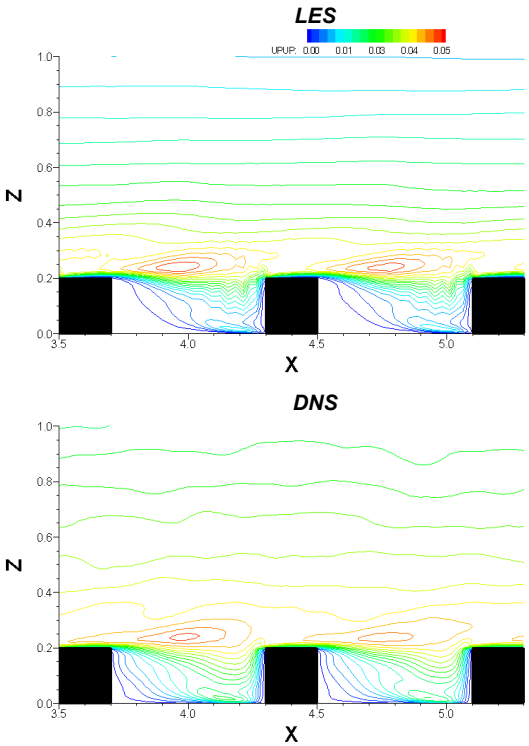

a.) quasi-smooth roughness

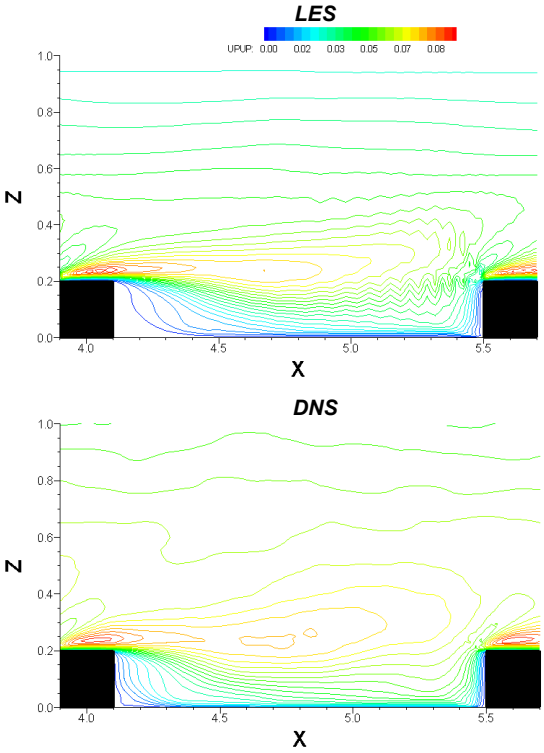

b.) transitional roughness

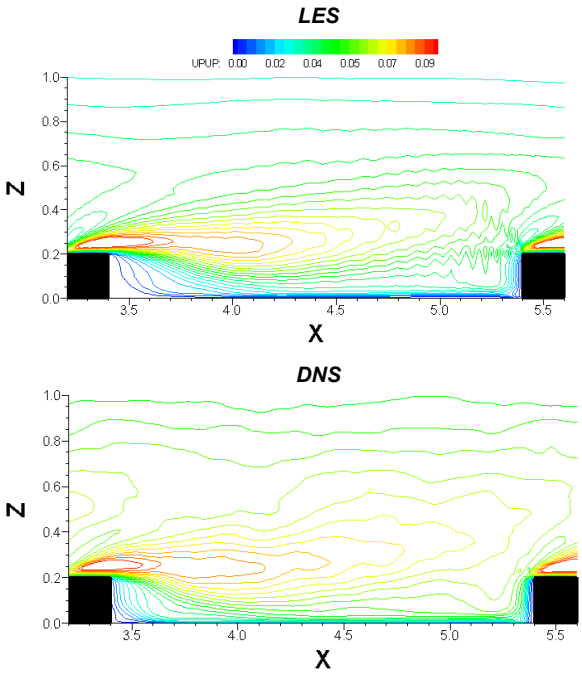

c.) isolated roughness

Figure 11-5 Comparison of LES and DNS results for the streamwise velocity fluctuations in the vicinity of the square bars for the three roughness types

However, in the centre of the channel the fluctuations are generally underestimated. This reflects the rather coarse resolution (the grid is refined near the walls) in this area, such that only the large scale fluctuations are resolved.

11.4.1 Instantaneous Flow Field

Figure 11-6 shows distributions of the instantaneous streamwise velocity fluctuation *u'*, together with the fluctuation velocity vectors (*u'-w'*) in an x-z plane. The vectors illustrate the presence of vortical motion, especially near the elements. The blue and red patches indicate fluid that moves faster (red) or slower (blue) than the mean flow.

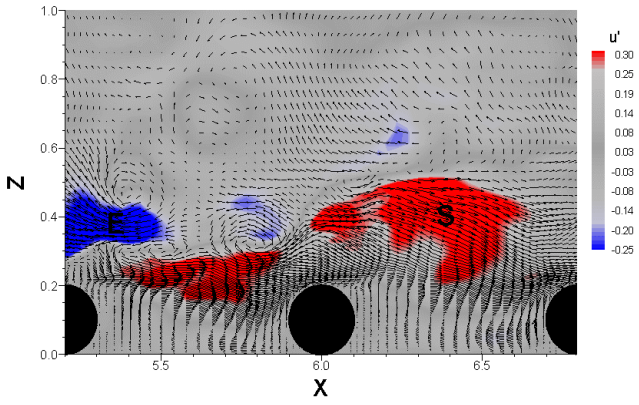

a.) quasi-smooth roughness

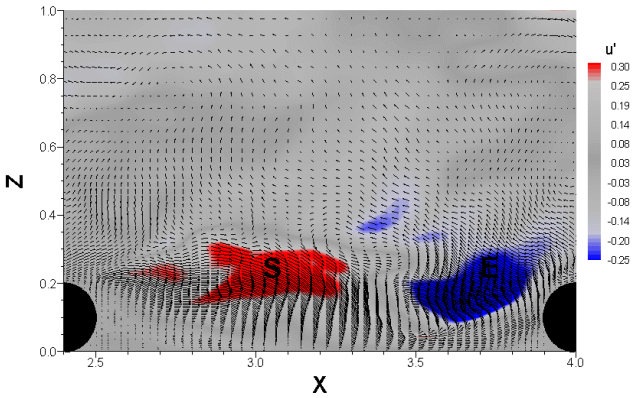

b.) transitional roughness

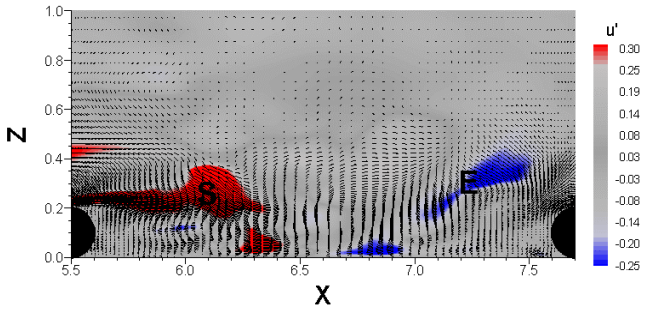

c.) isolated roughness

Figure 11-6 Distribution of streamwise perturbation (coloured) together with the perturbation vector (u',w') in the vicinity of the rods for the three roughness types

Above the crests of the roughness elements, sweeps, with faster fluid being pushed towards the wall and ejections, with slower fluid being expelled away from the wall, can be detected. These events are dominant near the wall irrespective of roughness type and roughness form. The decay of the turbulent motions towards the centre of the channel is also clearly visible.

The turbulent boundary layer over a smooth wall is characterized by alternating high and low speed streaks, which lift up and break down during a burst cycle (see e.g. /Kline et al. 1967/, /Robinson 1991/). For the rough wall cases, streaky structures are also present just above the roughness elements as was shown by /Djenidi et al. 1999/ in a laboratory experiment with the help of dye. Figure 11-7 shows instantaneous distributions of *u'* in a x-y plane just above the bars for the three roughness configurations and, for comparison, near the smooth wall. Here, the presence of coherent high speed (indicated by the red colour) and low speed (blue colour) streaks alternating in the spanwise direction are visible. By increasing the spacing between the bars, the strength of these streaks increases, which is due to increased momentum exchange with the outer layer. This is in accordance with observations from a quadrant analysis by /Krogstadt & Antonia 1994/. Furthermore, with an increase in the ratio of *w/k* the form of these streaks changes. While near the smooth wall the streaks are elongated, they are shorter and wider for the quasi-smooth, isolated and transitional roughness. However, the streak spacing seems to be constant irrespective of roughness type.

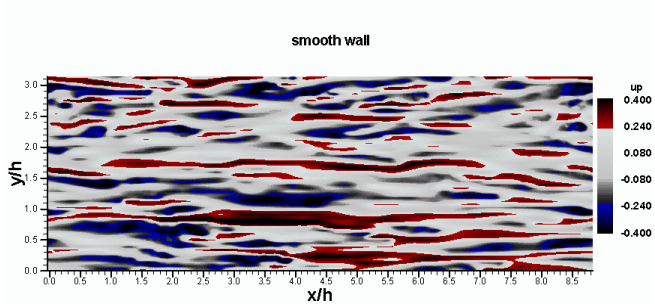

a) smooth wall

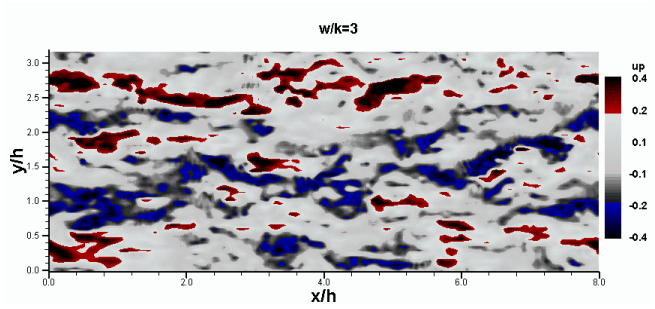

b.) quasi-smooth roughness

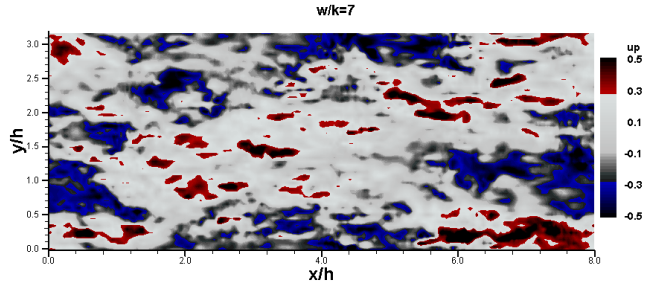

c.) transitional roughness

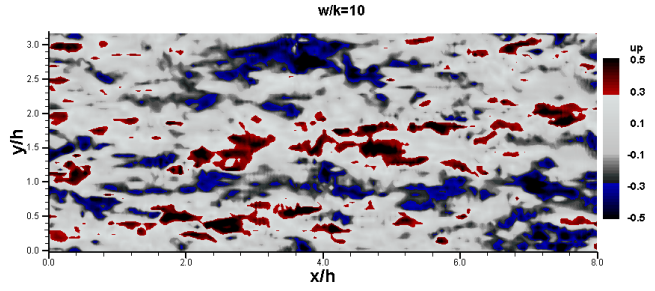

d.) isolated roughness

Figure 11-7 High and low speed streaks near the smooth upper wall (a) and above the elements for the three roughness configurations (b. – d.)

11.5 Conclusions

In this paper we have presented the results of large eddy simulations of closed channel flow over artificially roughened channel beds for the three

roughness types: isolated, wake interference, quasi-smooth roughness. Instantaneous and mean separation and recirculation as well as outflow from and inflow into the cavities are shown to occur for all roughness types. As a result turbulent fluctuations and Reynolds stresses are increased above the rough wall compared to values over a smooth wall. An important role plays the nature of the roughness, being responsible for the magnitude of the stresses and the distribution of all turbulent quantities in the entire flow. This supports the statement of /Djenidi et al. 1999/ who underline the inadequacy of a roughness classification scheme based solely on the effect the roughness has on the mean velocity profile. The present study has shown that the type of roughness is of significance especially in the formation of near wall coherent structures. Although streaks form above all types of roughness, their size and shape are different for each roughness configuration.

11.6 Literature

Antonia, R. A. 1994

The Effect of Different Types of Surface Conditions on a Turbulent Boundary Layer. 1st Intern. Conference on Flow Interaction. Ed. N.W.M. Ko & B.H.K. Lee. Pp 64 – 97

Breuer, M. & Rodi, W. 1996

Large Eddy Simulation of Complex Turbulent Flows of Practical Interest. In: Notes on Numerical Fluid Mech., Flow Simulations with High Performance Computers II. Ed.: Hirschel, E. H. Vieweg, Braunschweig. pp 258-274

Corino, E.R. & Brodkey, R.S. 1969

A Visual Investigation of the Wall Region in Turbulent Flow. J. Fluid Mech. Vol. 37, No. 1. pp 1-30

Defina, A. 1996

Transverse Spacing of Low-speed Streaks in a Channel Flow Over a Rough Bed. In: Coherent Flow Structures in Open Channels. Ed.: Ashworth, P. J., et Al. Wiley, New York

Djenidi, L.; Elavarasan, R.; Antonia, R. A. 1999

The Turbulent Boundary Layer Over Transverse Square Cavities. J. Fluid Mech., Vol. 395, pp 271 – 294

Germano, M.; Piomelli, U.; Moin, P.; Cabot, W.H. 1991

A Dynamic Subgrid-Scale Eddy Viscosity Model. Physics Fluids. Vol. 3. pp 1760-1765

Grass, A.J. 1971

Structural Features of Turbulent Flow Over Smooth and Rough Boundaries. J. Fluid Mech. No. 50(2). pp 233-255

Grass, A.J.; Stuart, R.J.; Mansour-Tehrani, M. 1991

Vortical Structures and Coherent Motion in Turbulent Flow Over Smooth and Rough Boundaries. Philosophical Transactions Royal Society of London A. Vol. 336. pp 35-65

Kline, S. J.; Reynolds, W. C.; Schraub, F. A.; Rundstadler, P. W. 1967

The Structure of Turbulent Boundary Layers. J. Fluid Mech. No. 30. pp 741-773

Krogstadt, P. A. & Antonia, R. A. 1994

Structure of Turbulent Boundary Layers on Smooth and Rough Walls. J. Fluid Mechanics. Vol. 245. pp 599 – 617

Leonardi, S.; Orlandi, P.; Djenidi, L.; Antonia, A. 2003

Structure of Turbulent Channel Flow with Square Bars on One Wall. Proceedings TSFP-3. Sendai, Japan, 24-27 June 2003

Lu, S. & Willmarth, W. W. 1973

Measurements of the Structure of Reynolds Stress in a Turbulent Boundary Layer. J. Fluid Mech. No. 60. pp 481-571

Miyake, Y.; Tsujimoto, K.; Nagai, N. 2002

Numerical Simulation of Channel Flow with a Rib-roughened Wall. J. of Turbulence. Vol. 3. pp 1-17

Morris, H.M. 1955

Flow in rough conduits. ASCE Transactions, Vol. 120, Paper No. 2745, 373-410

Nakagawa, H. Y. & Nezu, I. 1977

Prediction Of The Contribution To Reynolds Stress From Bursting Events In Open-Channel Flows. J. Fluid Mech.. Vol. 80 (1). pp. 99-128

Patel, V.C. 1998

Perspective Flow at High Reynolds Number and Over Rough Surfaces - Achilles Heel Of CFD. ASME J. Fluids Engineering. Vol. 120. pp 434-444

Perry, A. E, Schofield, W. H, Joubert, P. N. 1969

Rough Wall Turbulent Boundary Layers. J. Fluid Mech., Vol. 37, pp.383-413

Peskin, C.S. 1972

Flow Patterns Around Heart Valves: a Numerical Method. Journal of Computational Physics, Vol. 10, pp. 252-271

Raupach, M.R. 1981

Conditional Statistics of Reynolds Stress in Rough-Wall and Smooth-Wall Turbulent Boundary Layers. J. Fluid Mech. Vol. 108. pp 363-382

Robinson, K. 1991

Coherent Motions in the Turbulent Boundary Layer, Ann. Rev. Fluid Mech. Vol. 23. pp 601-639

Stone, H.L. 1968

Iterative Solution of Implicit Approximation of Multi-dimensional Partial Differential Equations. SIAM J. Numerical Analysis. No. 3

Tremblay, F. & Friedrich, R. 2001

An algorithm to Treat Flows Bounded by Arbitrarily Shaped Surfaces with Cartesian Meshes. In: Notes on Numerical Fluid Mechanics, Vol. 77, Springer

Verzicco, R.; Mohd-Yusof, J.; Orlandi, P.; Haworth, D. 2000

Large Eddy Simulation in Complex Geometric Configurations Using Boundary Body Forces. AIAA Journal, Vol. 38, No. 3, pp. 427-433